ISSN: 0974-5823 Vol. 7 No. 2 February, 2022

International Journal of Mechanical Engineering

Kinematic validation of an intact L4-L5 spinal unit finite element model constructed from an educational model

Suhaib Yaroub Al-Rubaie

Department of Biomedical Engineering, College of Engineering, Al-Nahrain University, Baghdad, Iraq

Sadiq Jaffar Hamandi

Department of Biomedical Engineering, College of Engineering, Al-Nahrain University, Baghdad, Iraq

Khaleel Ibraheem Mohson

Iraqi National Cancer Research Center, University of Baghdad, Baghdad, Iraq

Abstract

Purpose: This work aims to establish and validate a healthy model for the 4th and 5th lumbar vertebrae functional spinal unit intended for biomechanical analysis.

Methods: Towards that goal, a computed tomography scan to an educational 4th and 5th lumbar vertebrae model was conducted in order to reconstruct a three-dimensional model. The model consisted of two vertebrae divided into three bony parts (cortical, cancellous, and posterior element), endplates, intervertebral disc (nucleus pulposus and annulus fibrosus), and five ligaments. The material properties were assigned and the loading and boundary conditions were identical to the in-vitro biomechanical experiments. Additionally, mesh convergence was also conducted. Flexion, extension, lateral bending, and rotation motions were simulated and the ranges of motion were compared with cadaveric test and computational data from the existing literature.

Results: The results of the finite element model were consistent with the in-vitro experiments and validated finite element models from previously published data, validating the accuracy of the model.

Conclusions: The model built in this study is reliable, and effective and can be used in modeling different spinal movements, pathological cases, and implanted devices in future biomechanical simulations.

Keywords

biomechanics, kinematics, lumbar spine, 3D model, finite element method, validation

Introduction

The biomechanics of the lumbar spine is both structurally and functionally complex. It has to provide a wide complex physiological range of motion (RoM) while allowing load transfer [1]. Therefore, understanding biomechanics is essential to prevent injury and development in surgical techniques and implants. The finite element method (FEM) can be used as an effective way to study the lumbar spine biomechanics without the ethical concerns, difficulties, and limitations associated with physical experimentation, while providing detailed information about displacements, RoM, and stress-strain distribution in a functional spinal unit (FSU) [2]. However, validation of finite element (FE) models is essential to ensure the modeled system response correctly represents the actual system [3].

In the past decades, lumbar spine researches can be divided into clinical/experimental (in-vivo and in-vitro), along with computational (in-silico) biomechanical studies. In-vivo studies take advantage of several radiographic devices and techniques to investigate the mobility of the lumbar spine globally or segmentally [4]-[7]. Nevertheless, methods utilized in these researches have various limitations including varying physiological loading conditions and quantifying techniques. In-vitro studies commonly perform experiments on cadavers to predict the kinematics of the spine. These experiments are recognized as gold standards in RoM assessment [8]-[11]. Lastly, in-silico studies incorporate the use of the FEM for the examination of the lumbar spine biomechanics. Most of the lumbar spine finite FE models were patient-specific models developed from a computed tomographic (CT) scan of a cadaver or volunteer and either for the entire lumbar spine (5 FSU) or single FSU [12]-[22].

Therefore, the FEM and a realistic educational model for the 4th and 5th lumbar vertebrae (L4-L5) FSU were used in this study. The use of such a method saves significant effort and eliminates the requirement for the CT imaging of volunteers. Thus, the objectives of this study were to build a healthy nonlinear three-dimensional (3D) FE model of the L4-L5 FSU from a CT scan of an educational spinal model. Then verify model mesh convergence with the optimum element size and finally validate the model by

comparing the RoM of the model with data obtained by mechanical testing of human cadaver specimens in-vitro and FE studies. The validation of this study will serve as a fundamental point for future FE models with different spinal disorders. In addition, this work is a step toward the development of a clinical tool for investigating the biomechanics of patients with lumbar spondylolisthesis.

Materials and methods

Imaging and modeling

A CT scan (Ingenuity Core, Philips Medical System) with a thickness of 0.8 mm (0.4 mm increment) of an intact realistic educational L4-L5 spinal model (Classic LxH Dynamic Disc Model, Dynamic Disc Designs Corp.) was used to obtain the geometric information and reconstruct a 3D model of L4-L5 FSU. The anatomical details of the model were listed in Table 1.

Table 1. Anatomical dimensions of the L4-L5 educational model compared to literature data.

		VBH(A) (mm)	VBH (C) (mm)	VBH (P) (mm)	VBD (mm)	VBW (mm)	IVDH (mm)	Segmental angle (°)
This study	L4	28.37	23.45	25.05	32.83	40.27	(A) 11.5 (C) 10.13 (P) 9.66	13.4°
	L5	27.84	22.28	24.3	36.46	44.05		
In-vitro n:6 [14]	L4	27.8 (2.4)	24.1 (3.4)	28.0 (2.1)	-	-	12.7 (2.6)	-
	L5	29.5 (1.4)	25.3 (1.8)	24.9 (3.8)				
In-vivo n:59 [16]	-	-	-	-	-	-	-	13.4±7.9°
FEM [13]	L4	24.1 ± 3.81			-	-	11.3±0.3	-
	L5	22.9 ± 3.46						
FEM [20]	L4	27			33.7	50.3	12.8	-
	L5	24.3			35.8	53.3		

n: sample size; VBH: vertebral body height; VBD: vertebral body depth; VBW: vertebral body width; IVDH: intervertebral disc height; A: anterior; C: central; P: posterior.

The digital imaging and communications in medicine (DICOM) images were imported into 3D Slicer software (version: 4.13.0). The segmentation of the L4 and L5 vertebrae (anterior and posterior parts) and the intervertebral disc (IVD) were carried out using the threshold tool and further refinement was done using paint and erase tools. Cortical and cancellous bone was separated with shrink and logical operation tools. The thickness of the cortical bone was set to 0.6 mm [23]. The IVD was generated from the contour of endplates and divided with the scissors tool into nucleus pulposus (NP) (44% of the IVD volume) and surrounded by annulus fibrosus (AF) (56% of the IVD volume) and the NP was shifted 1.5 mm posteriorly [17], [24], [25]. The same previous tool was used to add the cartilaginous endplates between the vertebrae and IVD and the major vertebral ligaments (anterior longitudinal ligament (ALL), posterior longitudinal ligament (PLL), ligamentum flavum ligament (LF), supraspinous ligament (SSL), and interspinous ligament (ISL).

As shown in Fig. 1, the final model consisted of two cortical bones, two cancellous bones, two vertebral arches, two endplates, NP and AF, and the major ligaments. Before exporting the surface model, it was smoothed to remove defects including holes, artifacts, and rough edges and exported as 15 files for each segment. The stereolithography (STL) files were opened using SpaceClaim software (SpaceClaim 2020 R1, ANSYS, Inc) in order to convert them into solid geometric models using the reverse engineering method to be opened by the FE software.

Material properties

The material parameters of those mentioned model components are shown in Table 2, as referenced from previous reports [21], [26]-[30]. And the major ligaments were modeled using geometric data taken from previous studies and listed in the same table [27]. Bonded contact was used between model components, while contact between facet joints was assumed to be a frictionless contact.

Both the anterior and posterior vertebral parts were modeled as a linear elastic material because daily loading conditions were simulated. Under these loads, the bone material can be simplified to behave linearly with the change of the load [23]. Due to the heterogeneous anisotropic nature of the IVD, the material properties of the AF were selected to best fit the experimental data [31].

For flexion, extension, lateral bending, and axial rotation movements, the AF of the IVD was modeled using a non-linear hyperelastic material called the Mooney- Rivlin model [21], [26]-[29]. While it was modeled as a linear material for the compression load [30]. The NP was modeled as an incompressible linear or Mooney-Rivlin material for compression and rotation movement, respectively [27], [30]. The ligaments were modeled as 3D elements with multi-linear mechanical properties [28]. As ligaments resist tension only, they were only included in the analysis when they were subjected to tension load ((PLL, LF, ISL, and SSL) in flexion, (ALL and SSL) in extension, SSL in lateral bending, and no ligament in axial rotation) [10].

Table 2. Material properties and geometrical parameters used in the FE analysis.

		Element type	Young's modules (MPa)	Poisson ratio	Element size (mm)	Area (mm^2)	Reference
Cortical bone		Isotropic, elastic	12000	0.3	1.0	-	[26]-[28]
Cancellous bone			100	0.2	2.0		
Posterior bone			3500	0.25	1.5		[26], [27]
Endplate			24	0.4	1.0		[26], [29]
AF	Compression		4.2	0.45	0.5		[30]
	Flexion-extension	Mooney-Rivlin	C10 0.18; C01 0.045; D 1				[27]-[29]
	Bending and rotation		C10 0.56; C01 0.14; D 1				[21], [26]
NP	Compression	Isotropic, elastic	0.2	0.4999	1.0		[29], [30]
	Flexion-extension, bending, and rotation	Mooney-Rivlin	C10 0.12; C01 0.03; D 1				[27]-[29]
ALL		Multi linear	347 (ε<12.2) 787 (12.2<ε<20.3) 1864 (20.3<ε)	0.3	1.5	63.7	[27], [28]
PLL			29.5 (ε<11.1) 61.7 (11.1<ε<23) 236 (23<ε)			20	
LF			7.7 (ε<5.9) 9.6 (5.9<ε<49) 58.2 (49<ε)			40	
ISL			1.4 (ε<13.9) 1.5 (13.9<ε<20) 14.7(20<ε)			40	
SSL			2.5 (ε<20) 5.3 (20<ε<25) 34 (25<ε)			30	

Meshing

All the model components were meshed with first-order tetrahedral elements and a mesh convergence analysis was performed in ANSYS (ANSYS 2020 R1, ANSYS, Inc.) to obtain optimum mesh size for FEM as it is an important factor for the simulation accuracy. Nine element sizes (0.2 mm - 2 mm) were used in this meshing sensitivity study.

A compression loading test was performed. The bottom of L5 was fully constrained and a uniformly distributed force of 1000 N was added to the upper surface of the L4 segment. The results of different mesh resolutions were compared, and those within < 5% were considered converged [32].

Loading and simulation

To evaluate the validity of the converged model, the L4-L5 FSU was loaded with 3 different loading conditions, applied to the superior surface of the L4 vertebral body, whereas the inferior surface of L5 was kinematically constrained at six degrees of freedom. The loading conditions were:

a) Axial compression with a maximum force of 1500 N,

b) A pure moment of 1, 2.5, 5, 7.5 and 10 Nm in three different orientations (flexion and extension, lateral bending, and axial rotation),

c) Similar to the previous condition but with a 500 N preload force for accounting of the effect of the bodyweight above L4 and the muscle forces [17], [25], [33]. The compression load direction was set to not create any additional rotation.

The simulations were set to replicate the experimental and numerical studies for the

compression and moment (with and without preload) conditions. All the mesh manipulation and simulation work were conducted using FE analysis software (ANSYS 2020 R1, ANSYS, Inc.) and implemented on a laptop computer with an Intel Core i7-9750H CPU and 24Gb RAM.

Results

Mesh convergence test

The results of the mesh convergence study are presented graphically in Fig. 2 for both maximum Von-Mises stress and displacement tetrahedral elements. The difference in Von-Mises stress between 0.5 mm and 0.4 mm was 4%, while the difference in the displacement for the same element sizes was 2%. If the meshing size is 0.3 mm, the improvement in Von-Mises stress and displacement accuracy (compared to 0.4 mm) would be 3.86% and 0.93%, respectively. However, this would lead to an increase in the computational cost by more than double.

Therefore, the IVD was meshed with 0.5 mm mesh density to yield an accurate solution and the rest of the model parts were meshed with element size between 1 and 1.5 mm to maintain an acceptable computation time. The final model consisted of 834,245 tetrahedral elements and 185,007 nodes.

FE model validation

Pure compression

Figure 3 shows a linear response of IVD displacement under a pure compression load. The maximum applied load was 1500 N with a displacement of 2.22 mm and the results were compared to published experimental and computational literature [8], [13], [18], [20], [21], [34], [35].

Pure moment

The RoMs for the applied pure moments of ±1 Nm, ±2.5 Nm, ±5 Nm, ±7.5 Nm, and ±10 Nm were presented in Fig. 4. The total flexion-extension, lateral bending, and axial rotation RoMs were 10.6°, 7.43°, and 3.05°, respectively. The total RoM for flexion-extension, lateral bending, and axial rotation were compared to the in-vitro experimental data and the validated FE models in the published literature [10], [13], [18], [20], [21], [33], [36], [37].

The angular rotation results for the L4-L5 FSU were plotted against the applied moment in Fig. 5. Under 10 Nm, the maximum flexion RoM was 5.7°, whereas the maximum extension result was 4.9°, yielding a total RoM of 10.6°. Maximum RoM for lateral bending and axial rotation were 7.43° and 3.05°, respectively. All three RoM curves demonstrated non-linear stiffening as the applied moment was increased. The flexion-extension motion displayed the most non-linearity, while the lateral bending results exhibited less stiffening for incremented moments. The lateral bending curve passed through the experimental and computational ranges at 5 Nm and showed slightly less curvature than both the experimental and computational curves.

Combined load

The 500 N pre-load angular rotations were also plotted against applied moment along with the pure moment data and compared to Weisse et al. [20] results as shown in Fig. 6. The maximum RoM with pre-load in flexion, extension, lateral bending, and axial rotation were 7.12°, 5.42°, 7.21°, and 2.7°, respectively. Both flexion and extension with pre-load curves were more flexible in comparison to the without pre-load curves. For flexion, the increases in the angular motion were 1.43°, 1.53°, 1.69°, 1.78°, and 1.71° for 1 Nm, 2.5 Nm, 5 Nm, 7.5 Nm, and 10 Nm, respectively. While for extension, the increases were 2.02°, 1.67°, 1.1°, 0.99°, and 0.56° for -1 Nm, -2.5 Nm, -5 Nm, -7.5 Nm, and -10 Nm, respectively. In lateral bending, the RoMs of both with and without pre-load were almost identical with similar curvature. The axial rotation motion results were stiffer compared to the pure moment results with differences ranging between 0.6° at 1 Nm and 1.5° at 10 Nm.

Discussion

In this study, the focus was to validate an L4-L5 FSU FE model developed from an intact educational spinal model for three loading conditions: pure-compression, pure-moment, and moment with pre-load. In general, the results showed that the model was capable of giving detailed quantitative information on the mechanical behavior of the spine. The displacement and rotations curves from the generated FE-model show good accuracy of the experimental kinematics measurements.

As shown in figure 3, the linear compression-displacement response was between

sample 1 and 2 from Arun et al. [8] and within the probabilistic FE study [13]. Also, the results were comparable to the FE models of previous publications [18], [20], [21], [34], [35].

For the flexion and extension RoMs of the developed model were agreed and within the ranges of the in-vitro Heuer et al. [10], FE probabilistic FE study, and the computational FE models [13], [18], [20], [21], [33], [36], [37]. The flexion response was more flexible than the extension response, which aligns with experimental observations. In the combined loading scenario, the RoMs of the model in both flexion and extension increased due to the effect of compression load and results were in good agreement with the FE study reported by Weisse et al. [20]. The lateral bending RoM was in agreement with the range proposed by both Heuer et al. [10], and the computational FE models for the pure moment except for the 10 Nm where the developed model overprotected both ranges and 7.5 Nm where it was out of the range compared to the range of the computational FE models only [18], [20], [21], [36]. Similarly, the axial rotation RoM under pure moment was in agreement with both the Heuer et al. [10], and FE models except for the 2.5 and 5 Nm where it was underpredicted compared to published FE models only [18], [20], [21], [36]. The RoMs of the combined load in both lateral bending and axial rotation also show a similar trend with the range reported by Weisse et al. [20]. The axial rotation RoM under 500 N load was reduced in comparison to the pure moment load results which agree with the data reported by Weisse et al. [20].

The difference in the results between the numerical and in vitro data was expected due to the morphological (disc height and cross-sectional, lordotic curvature, facet morphology, and ligaments area) and material properties (disc and ligaments behavior and specimens age) differences between different specimens and FE models and the differences in the experimental setups. Niemeyer et al. [38] estimated that the natural variability of the morphology may explain a variation in the flexion and extension RoM by nearly 4°, 3° in lateral bending and 1.5° in axial rotation. Furthermore, the L4-L5 disc height in the model was lesser than the average disc height reported in the literature (Table 2), which may have resulted in a lesser RoM.

Although the FE model has been validated especially for intervertebral kinematics, this study has some limitations. Only a single spine geometry was studied. Also, the vertebrae were assumed to be rigid, although in reality, they would deform under loading. Furthermore, the relative rotations were calculated based on the motion of the superior endplate of the vertebra which is different from the experimental setups. Future work will investigate complex loading scenarios to evaluate spinal biomechanics utilizing the accuracy of the modeling framework described in this paper.

Conclusion

The modeling method presented in this paper was valid for predicting the kinematics of the human lumbar spine. The validated FE model can be modified and used to analysis the biomechanics with different spinal physiological and pathological conditions. Consequently, making it possible to simulate the instability and hypermobility conditions of the lumbar spine such as spondylolisthesis.

Acknowledgments

The authors would like to thank Buratha Diagnostic Center for help in acquiring the CT scan used in this study.

References:

[1] Nikkhoo M., Cheng C.H., Wang J.L., Khoz Z., El-Rich M., Hebela N., Khalaf K., Development and validation of a geometrically personalized finite element model of the lower ligamentous cervical spine for clinical applications, Comput Biol Med, 2019, 109, DOI: 10.1016/J.COMPBIOMED.2019.04.010.

[2] Dreischarf M., Zander T., Shirazi-Adl A., Puttlitz C.M., Adam C.J., Chen C.S., Goel V.K., Kiapour A., Kim Y.H., Labus K.M., Little J.P., Park W.M., Wang Y.H., Wilke H.J., Rohlmann A., Schmidt H., Comparison of eight published static finite element models of the intact lumbar spine: predictive power of models improves when combined together, J Biomech, 2014, 47(8), DOI: 10.1016/J.JBIOMECH.2014.04.002.

[3] Mills M.J., Sarigul-Klijn N., Validation of an in vivo Medical Image-Based Young Human Lumbar Spine Finite Element Model, J Biomech Eng, 2018, 141(3), DOI: 10.1115/1.4042183.

[4] Berry D.B., Hernandez A., Onodera K., Ingram N., Ward S.R., Gombatto S.P., Lumbar spine angles and intervertebral disc characteristics with end-range positions in three planes of motion in healthy people using upright MRI, J Biomech, 2019, 89, DOI: 10.1016/J.JBIOMECH.2019.04.020.

[5] Liu N., Wood K.B., Schwab J.H., Cha T.D., Pedlow F.X. Jr., Puhkan R.D., Hyzog T.L., Utility of Flexion-Extension Radiographs in Lumbar Spondylolisthesis: A Prospective Study, Spine J, 2015, 40(16), DOI: 10.1097/BRS.0000000000000941.

[6] Ochia R.S., Inoue N., Renner S.M., Lorenz E.P., Lim T.H., Andersson G.B., An H.S., Three-dimensional in vivo measurement of lumbar spine segmental motion, Spine J, 2006, 31(18), DOI: 10.1097/01.BRS.0000231435.55842.9E.

[7] Phan K.H., Daubs M.D., Kupperman A.I., Scott T.P., Wang J.C., Kinematic analysis of diseased and adjacent segments in degenerative lumbar spondylolisthesis, Spine J, 2015, 15(2), DOI: 10.1016/J.SPINEE.2014.08.453.

[8] Arun M.W.J., Hadagali P., Driesslein K., Curry W., Yoganandan N., Pintar F.A., Biomechanics of Lumbar Motion-Segments in Dynamic Compression, Stapp Car Crash J, 2017, 61, DOI: 10.4271/2017-22-0001.

[9] Heuer F., Schmidt H., Claes L., Wilke H.J., Stepwise reduction of functional spinal structures increase vertebral translation and intradiscal pressure. J Biomech, 2007, 40(4), DOI: 10.1016/J.JBIOMECH.2006.03.016.

[10] Heuer F., Schmidt H., Klezl Z., Claes L., Wilke H.J., Stepwise reduction of functional spinal structures increase range of motion and change lordosis angle, J Biomech, 2007, 40(2), DOI: 10.1016/J.JBIOMECH.2006.01.007.

[11] Panjabi M.M., Oxland T.R., Yamamoto I., Crisco J.J., Mechanical behavior of the human lumbar and lumbosacral spine as shown by three-dimensional load-displacement curves, J Bone Joint Surg Am, 1994, 76(3), DOI: 10.2106/00004623-199403000-00012.

[12] Affolter C., Kedzierska J., Vielma T., Weisse B., Aiyangar A., Estimating lumbar passive stiffness behaviour from subject-specific finite element models and in vivo 6DOF kinematics, J Biomech, 2020, 102, DOI: 10.1016/J.JBIOMECH.2020.109681.

[13] Bashkuev M., Reitmaier S., Schmidt H., Is the sheep a suitable model to study the mechanical alterations of disc degeneration in humans? A probabilistic finite element model study, J Biomech, 2019, 84, DOI: 10.1016/J.JBIOMECH.2018.12.042.

[14] Busscher I., Ploegmakers J.J.W., Verkerke G.J., Veldhuizen A.G., Comparative anatomical dimensions of the complete human and porcine spine, Eur Spine J, 2010, 19(7), DOI: 10.1007/S00586-010-1326-9.

[15] Finley S.M., Brodke D.S., Spina N.T., DeDen C.A., Ellis B.J., FEBio finite element models of the human lumbar spine, Comput Methods Biomech Biomed Engin, 2018, 21(6), DOI: 10.1080/10255842.2018.1478967.

[16] Han S.H., Hyun S.J., Jahng T.A., Kim K.J., A Comparative Radiographic Analysis of Fusion Rate between L4-5 and L5-S1 in a Single Level Posterior Lumbar Interbody Fusion. Korean J Spine J, 2015, 12(2), DOI: 10.14245/KJS.2015.12.2.60.

[17] Naserkhaki S., Arjmand N., Shirazi-Adl A., Farahmand F., El-Rich M., Effects of eight different ligament property datasets on biomechanics of a lumbar L4-L5 finite element model, J Biomech, 2018, 70, DOI: 10.1016/J.JBIOMECH.2017.05.003.

[18] Remus R., Lipphaus A., Neumann M., Bender B., Calibration and validation of a novel hybrid model of the lumbosacral spine in ArtiSynth-The passive structures, PLoS One, 2021, 16(4), DOI: 10.1371/JOURNAL.PONE.0250456.

[19] Umale S., Yoganandan N., Kurpad S.N., Development and validation of osteoligamentous lumbar spine under complex loading conditions: A step towards patient specific modeling, J Mech Behav Biomed Mater, 2020, 110, DOI: 10.1016/J.JMBBM.2020.103898.

[20] Weisse B., Aiyangar A.K., Affolter C., Gander R., Terrasi G.P., Ploeg H., Determination of the translational and rotational stiffnesses of an L4-L5 functional spinal unit using a specimen-specific finite element model, J Mech Behav Biomed Mater, 2012, 13, DOI: 10.1016/J.JMBBM.2012.04.002.

[21] Xiao Z., Wang L., Gong H., Zhu D., Zhang X., A non-linear finite element model of human L4-L5 lumbar spinal segment with three-dimensional solid element ligaments, Theor Appl Mech Lett, 2011, 1(6), DOI: 10.1063/2.1106401.

[22] Xu M., Yang J., Lieberman I.H., Haddas R., Lumbar spine finite element model for healthy subjects: development and validation, Comput Methods Biomech Biomed Engin, 2017, 20(1), DOI: 10.1080/10255842.2016.1193596.

[23] Peng Y., Du X., Huang L., Li J., Zhan R., Wang W., Xu B., Wu S., Peng C., Chen S., Optimizing bone cement stiffness for vertebroplasty through biomechanical effects analysis based on patient-specific three-dimensional finite element modeling, Med Biol Eng Comput, 2018, 56(11), DOI: 10.1007/S11517-018-1844-X.

[24] Liu T., El-Rich M., Effects of nucleus pulposus location on spinal loads and joint centers of rotation and reaction during forward flexion: A combined finite element and Musculoskeletal study, J Biomech, 2020, 104, DOI: 10.1016/J.JBIOMECH.2020.109740.

[25] Masni-Azian, Tanaka M., Biomechanical investigation on the influence of the regional material degeneration of an intervertebral disc in a lower lumbar spinal unit: A finite element study, Comput Biol Med, 2018, 98, DOI: 10.1016/J.COMPBIOMED.2018.05.010.

[26] Haddas R., Xu M., Lieberman I., Yang J., Finite Element Based-Analysis for Pre and Post Lumbar Fusion of Adult Degenerative Scoliosis Patients, Spine Deform, 2019, 7(4), DOI: 10.1016/J.JSPD.2018.11.008.

[27] Jiang S., Li W., Biomechanical study of proximal adjacent segment degeneration after posterior lumbar interbody fusion and fixation: a finite element analysis, J Orthop Surg Res, 2019, 14(1), DOI: 10.1186/S13018-019-1150-9.

[28] Ling Q., He E., Zhang H., lin H., Huang W., A novel narrow surface cage for full endoscopic oblique lateral lumbar interbody fusion: A finite element study, J Orthop Sci, 2019, 24(6), DOI: 10.1016/J.JOS.2019.08.013.

[29] Schmidt H., Heuer F., Drumm J., Klezl Z., Claes L., Wilke H.J., Application of a

calibration method provides more realistic results for a finite element model of a lumbar spinal segment, Clin Biomech, 2007, 22(4), DOI: 10.1016/J.CLINBIOMECH.2006.11.008.

[30] Tsouknidas A., Michailidis N., Savvakis S., Anagnostidis K., Bouzakis K.D., Kapetanos G., A finite element model technique to determine the mechanical response of a lumbar spine segment under complex loads, J Appl Biomech, 2012, 28(4), DOI: 10.1123/JAB.28.4.448.

[31] Jacobs N.T., Cortes D.H., Peloquin J.M., Vresilovic E.J., Elliott D.M., Validation and application of an intervertebral disc finite element model utilizing independently constructed tissue-level constitutive formulations that are nonlinear, anisotropic, and time-dependent, J Biomech, 2014, 47(11), DOI: 10.1016/J.JBIOMECH.2014.06.008.

[32] Chuang W.H., Kuo Y.J., Lin S.C., Wang C.W., Chen S.H., Chen Y.J., Hwang J.R., Comparison among load-, ROM-, and displacement-controlled methods used in the lumbosacral nonlinear finite-element analysis, Spine J, 2013, 38(5), DOI: 10.1097/BRS.0B013E31828251F9.

[33] Schmidt H., Galbusera F., Rohlmann A., Zander T., Wilke H.J., Effect of multilevel lumbar disc arthroplasty on spine kinematics and facet joint loads in flexion and extension: a finite element analysis, Eur Spine J, 2012, 21, DOI: 10.1007/S00586-010-1382-1.

[34] Byrne R.M., Aiyangar A.K., Zhang X., Sensitivity of musculoskeletal model-based lumbar spinal loading estimates to type of kinematic input and passive stiffness properties, J Biomech, 2020, 102, DOI: 10.1016/J.JBIOMECH.2020.109659.

[35] Schmidt H., Galbusera F., Rohlmann A., Shirazi-Adl A., What have we learned from finite element model studies of lumbar intervertebral discs in the past four decades?, J Biomech, 2013, 46(14), DOI: 10.1016/J.JBIOMECH.2013.07.014.

[36] Jaramillo H.E., Gómez L., García J.J., A finite element model of the L4-L5-S1 human spine segment including the heterogeneity and anisotropy of the discs, Acta Bioeng Biomech, 2015, 17(2), DOI: 10.5277/ ABB-00046-2014-02.

[37] Rohlmann A., Zander T., Schmidt H., Wilke H.J., Bergmann G., Analysis of the

influence of disc degeneration on the mechanical behaviour of a lumbar motion segment using the finite element method, J Biomech, 2006, 39(13), DOI: 10.1016/J.JBIOMECH.2005.07.026.

[38] Niemeyer F., Wilke H.J., Schmidt H., Geometry strongly influences the response of numerical models of the lumbar spine—A probabilistic finite element analysis, J Biomech, 2012, 45(8), DOI: 10.1016/J.JBIOMECH.2012.02.021.

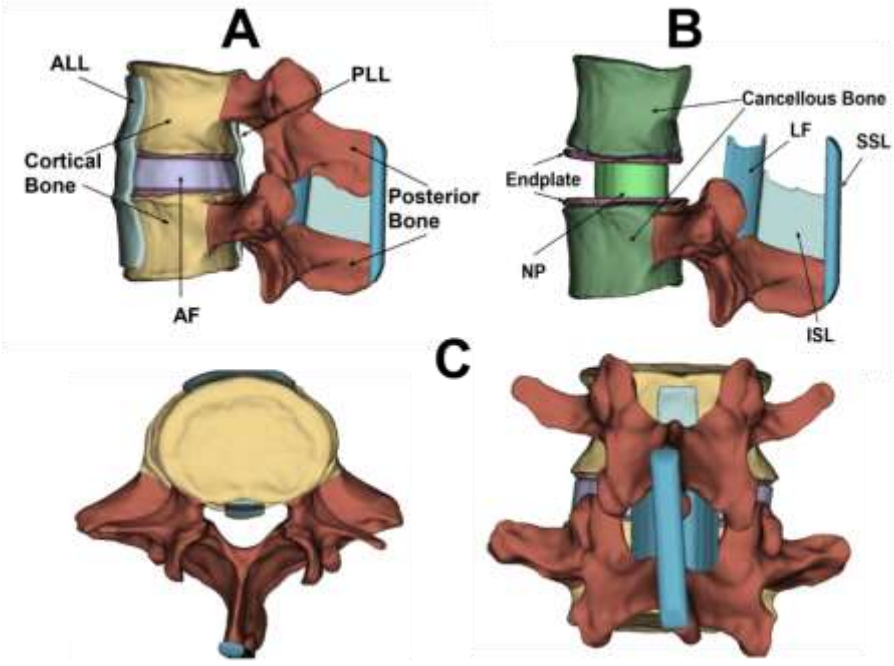

Fig. 1. A 3D intact L4-L5 FSU (A) complete model lateral view (B) parietal model showing candies bone, endplate, and NP (C) posterior and top views.

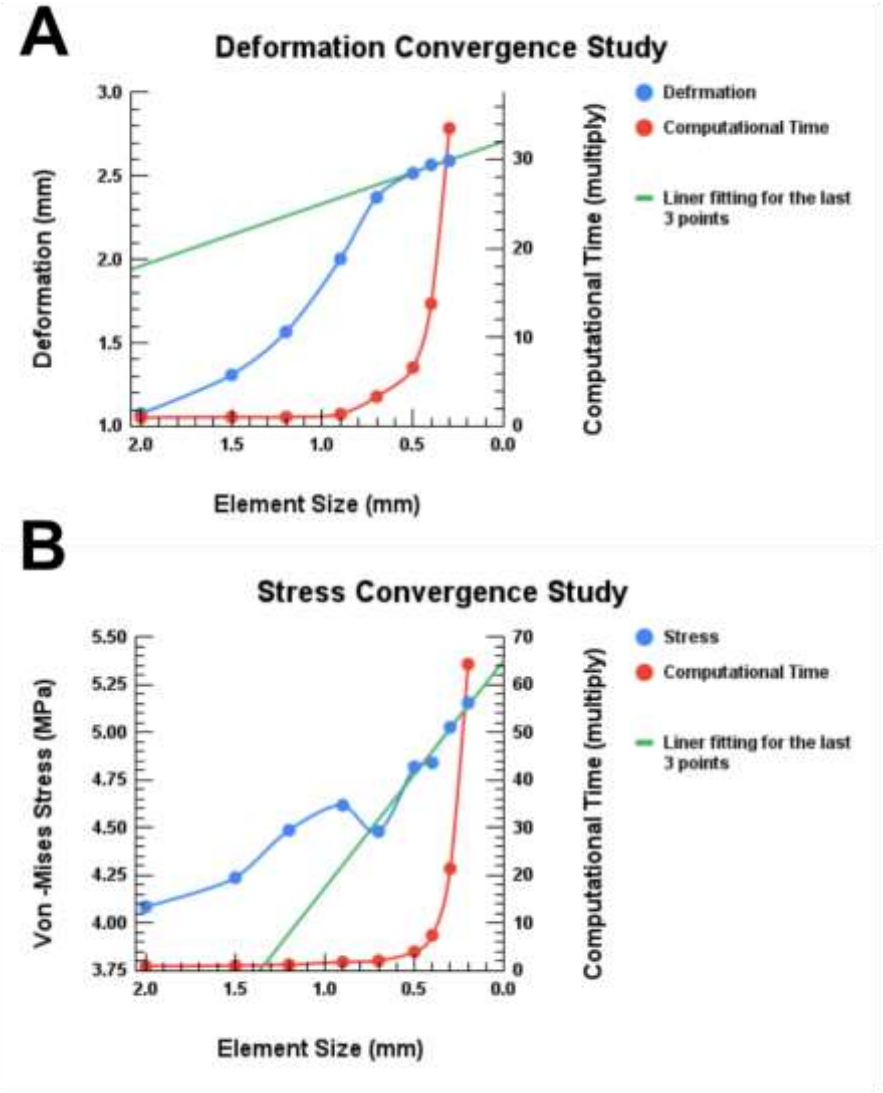

Fig. 2. Convergence study results show the effect of element size on (A) displacement, (B) Von-Mises stress. The second y-axes represent the computational time.

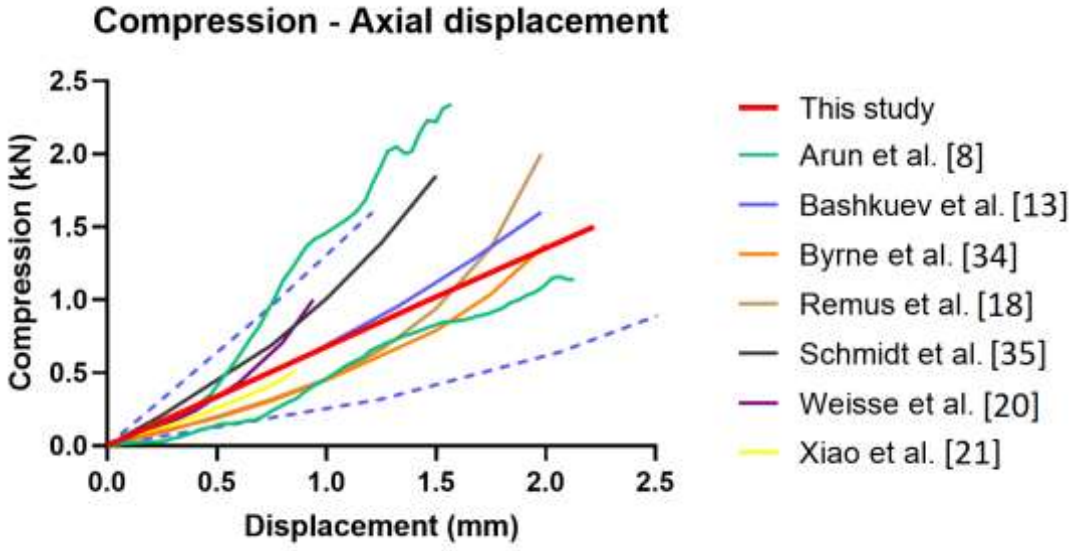

Fig. 3. Compression - axial displacement curve of present FE model and compared with previous studies.

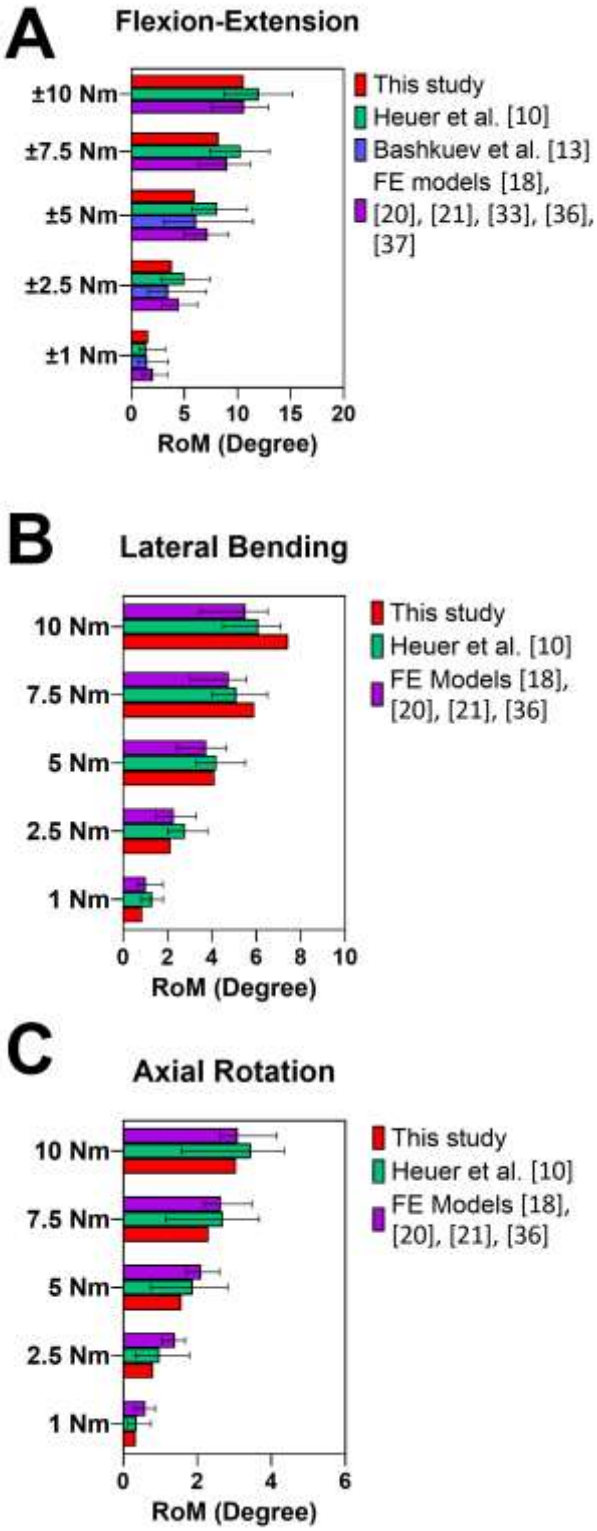

Fig. 4. Comparison of the RoM between the present FE model and previously published studies in (A) flexion-extension (B) lateral bending (C) axial rotation. The error bars indicate maximum/ minimum range.

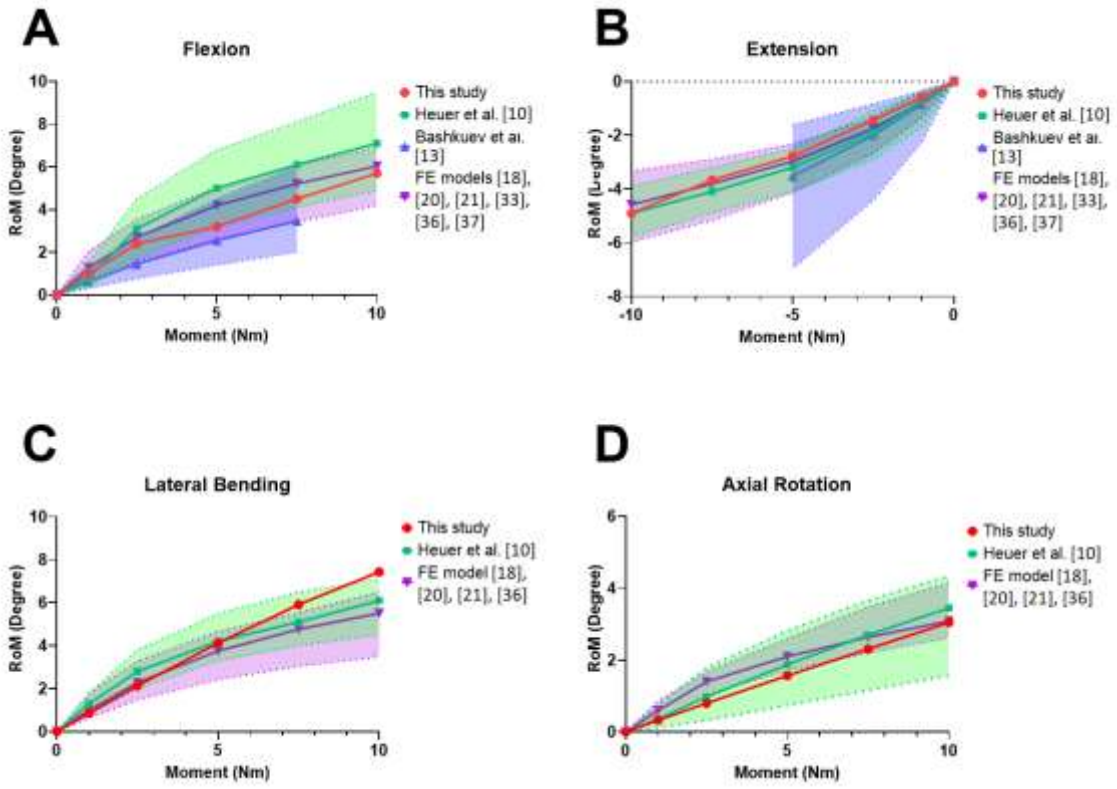

Fig. 5. Pure moment RoM curves of L4-L5 FSU in (A) flexion, (B) extension, (C) lateral bending, (D) axial rotation and compared to previously published data.

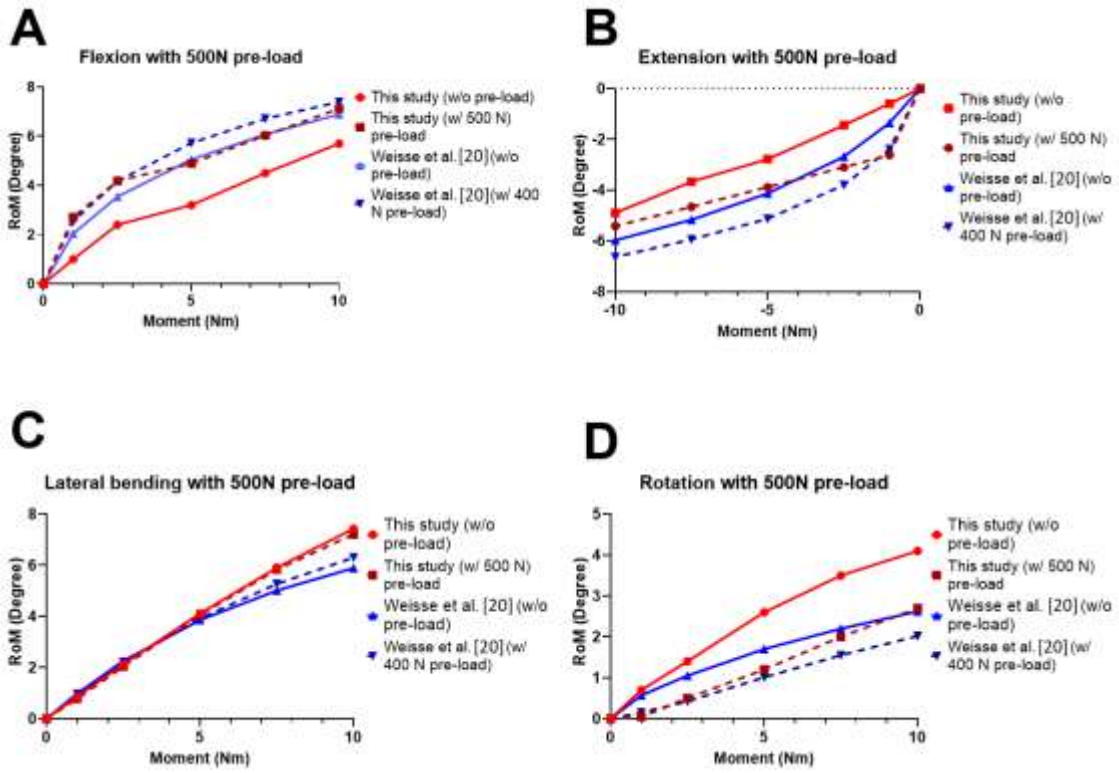

Fig. 6. Moment with pre-load RoM curves of L4-L5 FSU in (A) flexion, (B) extension, (C) lateral bending, (D) axial rotation and compared to previously published data.